



Article

Preparation of Nano-TiO₂-Coated SiO₂ Microsphere Composite Material and Evaluation of Its Self-Cleaning Property

Sijia Sun, Tongrong Deng, Hao Ding *, Ying Chen and Wanting Chen

Beijing Key Laboratory of Materials Utilization of Nonmetallic Minerals and Solid Wastes, National Laboratory of Mineral Materials, School of Materials Science and Technology, China University of Geosciences, Xueyuan Road, Haidian District, Beijing 100083, China; ssjcugb@163.com (S.S.); 18010157480@163.com (T.D.); chenying@cugb.edu.cn (Y.C.); wantingchen123@163.com (W.C.)

* Correspondence: dinghao@cugb.edu.cn; Tel.: +86-010-82322982

Received: 28 September 2017; Accepted: 30 October 2017; Published: 3 November 2017

Abstract: In order to improve the dispersion of nano-TiO₂ particles and enhance its self-cleaning properties, including photocatalytic degradation of pollutants and surface hydrophilicity, we prepared nano-TiO₂-coated SiO₂ microsphere composite self-cleaning materials (SiO₂-TiO₂) by co-grinding SiO₂ microspheres and TiO₂ soliquid and calcining the ground product. The structure, morphology, and self-cleaning properties of the SiO₂-TiO₂ were characterized. The characterization results showed that the degradation efficiency of methyl orange by SiO₂-TiO₂ was 97%, which was significantly higher than that obtained by pure nano-TiO₂. The minimum water contact angle of SiO₂-TiO₂ was 8°, indicating strong hydrophilicity and the good self-cleaning effect. The as-prepared SiO₂-TiO₂ was characterized by the nano-TiO₂ particles uniformly coated on the SiO₂ microspheres and distributed in the gap among the microspheres. The nano-TiO₂ particles were in an anatase phase with the particle size of 15–20 nm. The nano-TiO₂ particles were combined with SiO₂ microspheres via the dehydroxylation of hydroxyl groups on their surfaces.

Keywords: SiO₂; nano-TiO₂; self-cleaning; hydrophilicity

1. Introduction

Nano-titanium dioxide (TiO₂) is a typical semiconductor material with excellent properties. Moreover, it is stable, cheap, and non-toxic [1,2]. Therefore, it has been widely applied in the environmental protection [3], energy [4], and other fields [5,6]. In addition to the photocatalytic activity of TiO₂ under ultraviolet (UV) irradiation, the self-cleaning effect due to photoinduced hydrophilic properties of TiO₂ has always been one of the hotspots [7,8]. Its self-cleaning mechanism is generally ascribed to two effects [9,10]. Firstly, under the irradiation of ultraviolet light or ultraviolet in sunlight, the active components induced by the photocatalytic action of TiO₂ on the TiO₂ self-cleaning film can react with the pollutants adhering to the surface, thus achieving the decomposition of pollutants. Secondly, due to the super-hydrophilicity of the self-cleaning film, the decomposed products can be washed away by rain, so as to maintain the clean material surface [11]. In China and other developing countries, the contents of dust and oily dirt are high in the urban atmosphere and dust and oily dirt tend to adhere to building walls and glass surface to make the surface dirty. Nano-TiO₂ self-cleaning materials may be used to coat such surfaces [12,13].

However, some factors restrict the application scope of nano-TiO₂ self-cleaning materials. For example, the agglomeration phenomenon and poor dispersivity of TiO₂ particles in the application system significantly reduces its self-cleaning effect [14,15]. Coating TiO₂ particles on the matrix surface

can significantly improve the dispersibility of TiO₂ particles and enhance the photocatalytic efficiency and self-cleaning performance under the synergistic effect of the matrix [16,17]. In this way, the aforementioned problems may be solved. Many silicon materials are used as substrates to prepare nano-TiO₂ coated composite catalysts, such as quartz tube [18], glass fibers [19], and nano-silica [20]. These catalysts all exhibit the good photocatalytic activity with different functional characteristics. Meanwhile, the micro-nano-morphology of the carrier-based nanoparticles, which are constructed from the surface of the composite self-cleaning material, can also increase the roughness of the self-cleaning film and further improve the super-hydrophilic or super-hydrophobic properties [21,22] Prabhu [23] prepared the reduced graphene oxide (rGO)/TiO₂ composite self-cleaning material according to the solvothermal method and improved the visible light absorption efficiency of the composite self-cleaning materials, which exhibited the good photocatalytic efficiency and super-hydrophilic performance under light irradiation. Zhou [24] added the prepared SiO₂-TiO₂ composite colloidal particles into the fluorocarbon coating and realized more stable self-cleaning performance than that of adding single nano-TiO₂ particles under ultraviolet light irradiation, thus suggesting its possible industrial application in outdoor environments. Zhang [25] and Ciprian [26] prepared SiO₂-TiO₂ composite films by the sol-gel impregnation and freeze-drying deposition method and realized the excellent self-cleaning performance and high transmittance to visible light. In general, the abovementioned preparation methods of nano-TiO₂ composite self-cleaning material have some problems, such as the high cost, the complicated process and the difficulty in large-scale production and application. Therefore, it is necessary to select cheap matrix materials and simple composite process. Surolia [27] prepared the TiO₂-coated fly ash photocatalyst via the sol-gel method with the cheap fly ash as substrate, exhibiting well photocatalysis degradation performance. Therefore, it is an effective way to improve the efficiency of resource utilization by using natural mineral or industrial by-product as substrate to prepare nano-TiO₂-coated photocatalytic material.

In this study, with SiO₂ microspheres as the matrix, nano-TiO₂-coated SiO₂ microsphere composite self-cleaning materials (SiO₂-TiO₂) were prepared by the wet grinding of SiO₂ microspheres and nano-TiO₂ soliquid and the subsequent calcination of the ground product. Then, we determined the photocatalytic activity and photoinduced hydrophilicity of SiO₂-TiO₂, analyzed the structure and morphology, and discussed the mechanism of the interaction between TiO₂ and SiO₂ particles. The SiO₂ microspheres used in this study were recovered from the by-product, silica fume, which was produced during the industrial production of fused zirconia. The SiO₂ microspheres mainly exist in the amorphous phase and have regular morphology, high surface activity, and low cost [28,29]. However, during the past years, silica fume was usually applied in cement, concrete and refractory products as an additive and its use efficiency was low [30,31]. To the best of our knowledge, the preparation of functional materials including composite photocatalytic materials with SiO₂ microsphere as a matrix was seldom reported. In the study, the spherical shape of the SiO₂ microspheres can increase the fluidity of SiO₂-TiO₂ and promote the film formation process and the micrometer size of the SiO₂ can improve the recyclability of nano-TiO₂. It is expected that the SiO₂ microspheres can exert a synergistic effect on the performance of SiO₂-TiO₂ and reduce the cost of composite self-cleaning materials [25]. Meanwhile, the mechanical-chemical grinding method used in this study is a simple and non-pollution particle compound method. We prepared the SiO₂-TiO₂ composite materials with the good photocatalysis activity and self-cleaning effect via a simple composite process with cheap matrix materials. The preparation process exhibits significant economic and environmental values.

2. Methods

2.1. Raw Materials and Reagents

The SiO₂ microspheres used in this study were recovered from the by-product, silica fume, which was produced during the industrial production of fused zirconia and was provided by a zirconia production enterprise in Jiaozuo (Jiaozuo, China). The main chemical constituents (mass fraction, %)

of SiO₂ microspheres were 93.78% SiO₂ and 4.96% ZrO₂. SiO₂ is mainly composed of amorphous phase, exhibiting the microsphere morphology with the particle size of 1–3 μm. The SiO₂ particles are aggregated to form the aggregates with the larger particle size. After depolymerizing the aggregates, the SiO₂ microspheres exist in a dispersed state.

Tetrabutyl titanate (C₁₆H₃₆O₄Ti) from Beijing Chemical Industry Group Co., Ltd. (Beijing, China) was used as the titanium source. Acetylacetone (C₅H₈O₂) supplied by Xi Long Chemical Co., Ltd. (Guangzhou, China) was used as a hydrolysis control agent. Methyl orange (C₁₄H₁₄N₃SO₃Na) from Beijing Chemical Industry Group Co., Ltd. (Beijing, China) was used as a target pollution for photocatalytic degradation. Ethanol and deionized water are also used as solvents throughout the preparation process.

2.2. Preparation Method

2.2.1. Depolymerization of SiO₂ Microspheres

Considering the agglomeration effect of particles in the raw SiO₂ microspheres, SiO₂ microspheres need to be depolymerized and dispersed before compositing with nano-TiO₂. The depolymerization method was described as follows: The SiO₂ microsphere materials were added into the ethanol solution to form a suspension. After adding ceramic grinding balls (the ratio of ball to material, 3:1), the suspension was then ground in the mixing mill (CSDM-S3, Beijing Paleozoic Powder Technology Co., Ltd., Beijing, China) for 60 min. Finally, the dispersed SiO₂ microspheres were obtained after ball-material separation, filtration, and desiccation.

2.2.2. Preparation of Nano-TiO₂ Soliquid

Firstly, 8.5 mL of tetrabutyl titanate was dissolved into 10 mL of ethanol solution. The mixed solution was stirred evenly and marked as Solution A. Then, 1.3 mL of acetylacetone was dissolved into 10 mL of ethanol solution, and the obtained solution was marked as Solution B. Then, Solution B was slowly added into Solution A and 19.35 mL of the mixture of ethanol and water (water 0.85 mL) was also added into Solution A. Afterwards, the mixture was stirred vigorously at room temperature for 12 h and the stirred mixture was aged for 48 h to obtain the nano-TiO₂ soliquid. The viscosity of the nano-TiO₂ soliquid obtained after 48-h aging was measured to be 2×10^{-3} Pa·s by a digital display viscometer (NDJ-8S, Shanghai Precision Instrument and Meter Co., Ltd., Shanghai, China). For comparison, partial nano-TiO₂ soliquid was dried and calcined to prepare TiO₂ nanoparticles. According to the X-ray diffraction (XRD) data and the Scherrer Equation, the grain size of nano-TiO₂ was calculated to be 15–20 nm.

2.2.3. Preparation of SiO₂-TiO₂

Firstly, the dispersed SiO₂ microspheres were added into the ethanol solution, which was stirred to form a suspension. Secondly, the suspension was added into the aged nano-TiO₂ soliquid to form the SiO₂/TiO₂ mixture. Thirdly, the SiO₂/TiO₂ mixture were stirred by a CSDM-S3 mixing mill (Beijing Gosdel Powder&Technology Co., Ltd., Beijing, China) for 90 min after the addition of a certain amount of grinding balls to obtain the SiO₂/TiO₂ soliquid composites. Then, the SiO₂/TiO₂ soliquid composites were put in a SRJX-5-13 chamber electric furnace (Tianjin Taisite Instrument Co., LTD, Tianjin, China) and calcined at 500 °C for 2 h. Finally, the SiO₂-TiO₂ was prepared.

2.3. Characterization

2.3.1. Evaluation of Self-Cleaning Performance

Photocatalytic Activity

The photocatalytic degradation performance of SiO₂-TiO₂ was tested with the methyl orange as the target degradation pollutant. The system was irradiated by a mercury lamp (100 W, the main wavelength of 254 nm). Then, 40 mg of SiO₂-TiO₂ was added to 50 mL of prepared methyl orange dilution (concentration 10 mg/L). In order to reduce the measurement error caused by sample adsorption, the dark reaction was carried out for 0.5 h and then the concentration of methyl orange (C₀) in the solution was measured. After turning on the light source, the concentration of methyl orange (C) in solution was measured every 20 min. The photocatalytic degradation performance of the samples was characterized and evaluated based on the change of C/C₀.

The concentration of methyl orange was measured according to the following procedure. Firstly, the solution was centrifuged and the absorbance of the supernatant was measured with a Cary 5000 UV-VIS spectrophotometer (USA Varian, Palo Alto, CA, USA). The concentration of methyl orange in the solution was calculated according to the relationship between absorbance and concentration.

Hydrophilicity

The hydrophilicity of the SiO₂-TiO₂ particles was characterized based on the wetting degree of water on its surface. The wetting degree was reflected by the measured water contact angle on its surface. The SiO₂-TiO₂ composite powder was pressed into a sheet-like sample by a tableting machine and then the water contact angle was measured by a contact angle meter (JC2000D, Shanghai Zhongchen Digital Technic Apparatus Co. Ltd., Shanghai, China) three times. The measurement results were averaged.

2.3.2. Characterization of Structure and Morphology

We observed the morphology of SiO₂-TiO₂ by scanning electron microscope (SEM) (S-3500N, Hitachi, Ltd., Tokyo, Japan) and transmission electron microscope (TEM) (FEI Tecnai G2 F20, Portland, OR, USA). The surface functional groups were examined by an infrared spectroscope (Spectrum 100, PerkinElmer Instruments (Shanghai) Co., Ltd., Shanghai, China) with KBr as the medium, and the weights of each sample and KBr were, respectively, 1 and 200 mg. The phase analysis was carried out with an X-ray diffractometer (D/MAX2000, Rigaku Corporation, Tokyo, Japan). The specific surface areas of SiO₂ and SiO₂-TiO₂ were tested by the QuadraSorb SI specific surface area analyzer (Quantachrome Instrument Company, Boynton Beach, FL, USA). In addition, the surface roughness of SiO₂ microspheres and SiO₂-TiO₂ were evaluated using a Multimode VIII atomic force microscope (Bruker, Fremont, CA, USA).

3. Results and Discussion

3.1. Properties of SiO₂-TiO₂

3.1.1. Photocatalytic Properties of SiO₂-TiO₂

Figure 1a represents the degradation behaviors of methyl orange dye during irradiation as a function of time (min) in the presence of SiO₂-TiO₂ with different TiO₂ ratios (the mass ratio of TiO₂ to SiO₂-TiO₂). As shown in Figure 1a, the SiO₂ microspheres exhibit no degradation effect on methyl orange, whereas pure TiO₂ has a certain degradation effect on methyl orange. All of the prepared SiO₂-TiO₂ materials exhibit the significantly higher photocatalytic degradation efficiency on methyl orange dye than that of pure nano-TiO₂. Among these SiO₂-TiO₂ samples, with SiO₂-TiO₂-40 (TiO₂ ratio is 40%) as the photocatalyst, after the solution was irradiated for 40 min, the C/C₀ was

reduced to about 0.1 and the degradation efficiency reached 90%. After the 120 min irradiation, the degradation efficiency reached 97%. With the pure nano-TiO₂ as the photocatalyst, the degradation efficiencies after 40 and 120 min respectively reached 50% and 90%. The abovementioned results indicated that the photocatalytic activity of nano-TiO₂ had been greatly improved when TiO₂ coated the surface of SiO₂ microspheres. In addition, the TiO₂ ratio had a significant effect on the degradation efficiency of SiO₂-TiO₂. With the increase in the TiO₂ ratio from 20% to 40%, the photocatalytic degradation efficiency gradually increased and finally reached its maximum value. When the mass ratio of TiO₂ increased to 50%, the degradation efficiency decreased. However, the degradation efficiency of SiO₂-TiO₂ with different TiO₂ ratios was always higher than that of pure nano-TiO₂. The phenomenon might be interpreted in two aspects: Firstly, the coating of nano-TiO₂ on SiO₂ microsphere surface could improve the dispersibility of nano-TiO₂, thus resulting in an increase in the number of reactive groups under irradiation and increasing the quantum efficiency. Secondly, SiO₂ had a high reflection efficiency on ultraviolet radiation, and the light reflected by SiO₂ could be absorbed by TiO₂, thus improving the absorption of ultraviolet light by SiO₂-TiO₂. The specific surface area analysis results showed that the surface area of SiO₂ had been significantly increased from its original value of 5.698 to 44.410 m²/g after TiO₂ coating. This result also confirmed that the SiO₂ microspheres had been coated by nano TiO₂ effectively. Figure 1b shows the influence of the ratio of grinding ball to materials (B-M) in the grinding process on the photocatalytic activity of SiO₂-TiO₂. The degradation efficiency of SiO₂-TiO₂ samples prepared with grinding balls was significantly higher than that of the SiO₂-TiO₂ prepared without grinding balls (B-M is 0). The degradation effect was the best when the B-M ratio was 5. After 120 min irradiation, the highest degradation efficiency was 95% ($C/C_0 = 0.05$) at the B-M ratio of 5% and 65% at the B-M of 0. The above results showed that the grinding process had an important effect on the performance of SiO₂-TiO₂. Therefore, the proper B-M ratio should be selected. As shown in Figure 1b, the degradation effect of SiO₂-TiO₂ is stronger than that of pure nano-TiO₂. The result is consistent with the results shown in Figure 1a.

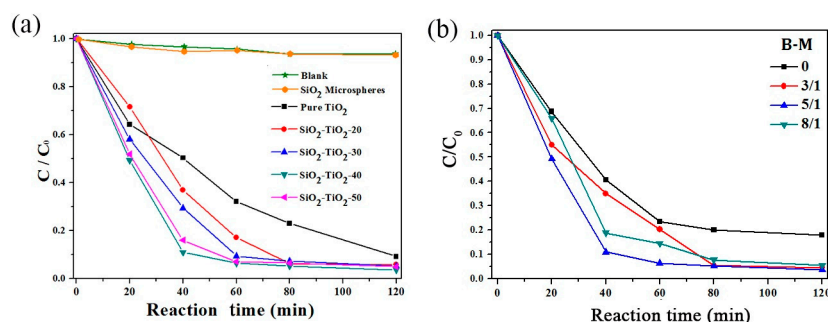


Figure 1. Influences of (a) TiO₂ ratio and (b) B-M ratio on the photocatalytic performance of SiO₂-TiO₂. (a) SiO₂-TiO₂-20, 30, 40, 50 represent the mass ratio of TiO₂ to SiO₂-TiO₂ is 20%, 30%, 40% and 50%; and (b) B-M represents the mass ratio of grinding balls to the materials.

The UV-VIS absorption spectra of bare SiO₂ microspheres, nano-TiO₂, and SiO₂-TiO₂-50 were obtained for comparison (Figure 2). The light absorption of SiO₂ in a wavelength range between 300 and 400 nm was insignificant, whereas TiO₂ absorbed light with the wavelength below 400 nm. The SiO₂-TiO₂ exhibited the higher light absorption in a wavelength range from 200 to 400 nm than that of pure nano-TiO₂, which was completely different from bare SiO₂ microspheres. The results indicated that the SiO₂-TiO₂ had the higher UV absorption due to the high reflection efficiency on ultraviolet radiation by SiO₂ microspheres, confirming that SiO₂ microspheres were coated by nano-TiO₂ particles with similar light absorption properties to TiO₂. Meanwhile, this results contribute to the good photocatalytic activity of SiO₂-TiO₂.

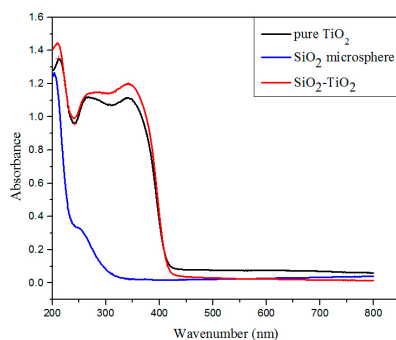


Figure 2. UV-VIS absorption spectra of pure TiO₂, SiO₂ microsphere and SiO₂-TiO₂.

3.1.2. Hydrophilic Properties of SiO₂-TiO₂

Figure 3 shows the change of water contact angle of SiO₂-TiO₂ particles with different TiO₂ ratios after irradiation by ultraviolet light for 2 h. For the SiO₂ microsphere materials, the contact angle was maintained to be 28° after UV irradiation, indicating that the UV light had no effect on its hydrophilicity. The water contact angle of pure TiO₂ is 26° before UV irradiation, which is higher than that of SiO₂-TiO₂, indicating that the coating of TiO₂ on SiO₂ surface can improve the hydrophilicity of TiO₂. The improvement effect may be interpreted as follows. The dispersion of nano-TiO₂ was improved and then more active hydroxyl groups on TiO₂ surface were exposed. Meanwhile, the water contact angle of pure TiO₂ decreased from 26° to 10° after UV irradiation, indicating the photoinduced hydrophilicity of TiO₂. The water contact angle of SiO₂-TiO₂ was 15–18° and decreased to 8–13° after UV irradiation, showing the strong hydrophilicity. The SiO₂-TiO₂-40 (TiO₂ ratio is 40) showed the strongest hydrophilicity and its water contact angles were 17° and 8° before and after UV irradiation respectively. The strong photo-induced hydrophilicity and photocatalytic activity of SiO₂-TiO₂ indicate its good self-cleaning performance.

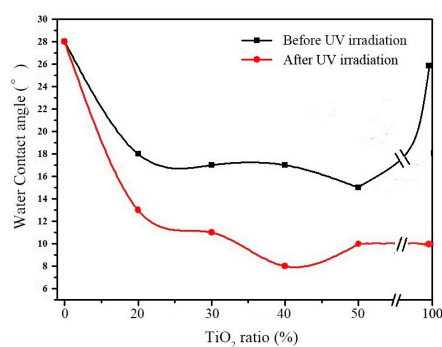


Figure 3. Relationship between the water contact angle and the content of TiO₂.

To investigate the mechanism of the photoinduced hydrophilicity of SiO₂-TiO₂, the infrared spectral analysis was carried out. Figure 4 shows the Fourier transform infrared spectroscopy (FT-IR) spectra of SiO₂-TiO₂-20 and SiO₂-TiO₂-30 before and after UV irradiation. The characteristic absorption peaks in the range of 2800–3800 cm⁻¹ and 1620 cm⁻¹ in all the samples were ascribed to the vibration of the hydroxyl groups on the SiO₂-TiO₂ surface. When the TiO₂ ratio was 30%, after the UV irradiation (b2 in Figure 4), the intensity of the absorption peak in the range of 2800–3800 cm⁻¹ in the FTIR spectrum of SiO₂-TiO₂ was higher than that in the spectrum b1 (before the UV irradiation) and the peak was shifted to the higher wavenumber. Meanwhile, the absorption peak at 1620 cm⁻¹ in b2 was sharper than that in b1. The abovementioned results indicated that the number of hydroxyl groups on the surface of SiO₂-TiO₂ increased after UV irradiation and that the SiO₂-TiO₂ exhibited the reaction activity with water. We believed that the production of hydroxyl groups was induced by

the photoinduced action of TiO_2 . The change was consistent with the remarkable enhancement of the surface hydrophilicity of $\text{SiO}_2\text{-TiO}_2$ after UV irradiation in Figure 3.

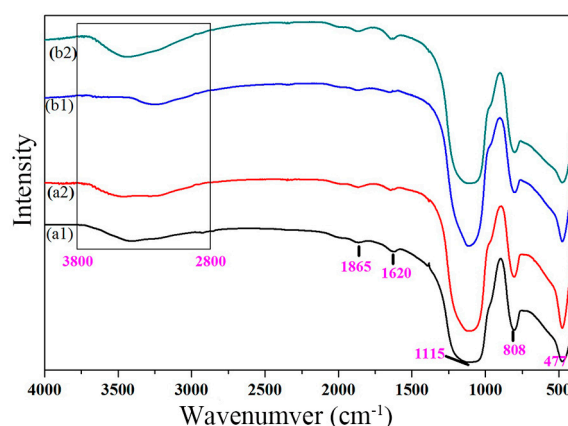


Figure 4. Fourier transform infrared spectroscopy (FT-IR) spectrum of the $\text{SiO}_2\text{-TiO}_2$ with different TiO_2 ratios. (a1) $\text{SiO}_2\text{-TiO}_2\text{-20}$, before UV irradiation; (a2) $\text{SiO}_2\text{-TiO}_2\text{-20}$, after UV irradiation; (b1) $\text{SiO}_2\text{-TiO}_2\text{-30}$, before UV irradiation; and (b2) $\text{SiO}_2\text{-TiO}_2\text{-30}$, after UV irradiation; The black rectangle region represents the absorption bands caused by the vibration of the hydroxyl radical

3.2. Structure and Morphology of $\text{SiO}_2\text{-TiO}_2$

3.2.1. XRD Analysis

Figure 5 shows the XRD patterns of $\text{SiO}_2\text{-TiO}_2$ with different TiO_2 ratios. In addition to the diffraction peak of amorphous SiO_2 microspheres, the diffraction peaks of the anatase phase also appeared in the XRD patterns of all $\text{SiO}_2\text{-TiO}_2$ samples, and the intensity of diffraction peaks of the anatase phase increased with the increase in the TiO_2 ratio. Especially, when the TiO_2 ratio was 50%, the complete anatase diffraction peak (JCPDS 21-1272) appeared in the XRD pattern of $\text{SiO}_2\text{-TiO}_2\text{-50}$ (Figure 5c) [32]. The abovementioned results indicated that nano- TiO_2 existed as an anatase phase. Among all the TiO_2 crystal phases, the anatase exhibited the highest photocatalytic activity, which was consistent with the results of photocatalytic activity and photoinduced hydrophilicity of $\text{SiO}_2\text{-TiO}_2$.

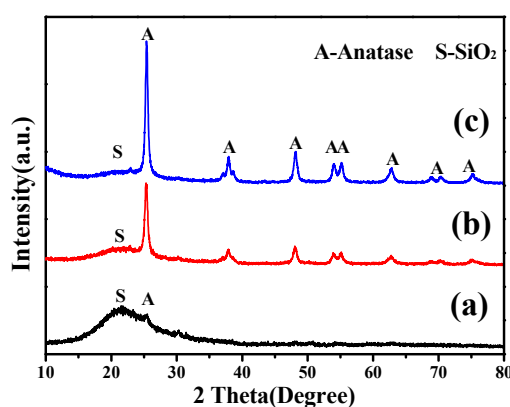


Figure 5. XRD patterns of $\text{SiO}_2\text{-TiO}_2$ with different TiO_2 ratios. (a) 30% TiO_2 ; (b) 40% TiO_2 ; and (c) 50% TiO_2 .

3.2.2. Morphology and Element Analysis

Figure 6 shows the SEM images of $\text{SiO}_2\text{-TiO}_2$ with different TiO_2 ratios. In Figure 6a, the exposed surfaces of SiO_2 microspheres are smooth without covering. However, the micron-submicron

hierarchical structure morphology can be observed in Figure 6b–d. The surface of the SiO₂ microspheres became rough and was covered with a certain amount of irregular particles. Meanwhile, with the increase in the TiO₂ ratio, the roughness and coverage area of the SiO₂ microsphere surface increased accordingly. According to the preparation process, it was presumed that the coating on the surface of the microspheres should be nano-TiO₂ particles. The surface roughness of SiO₂ microspheres and SiO₂-TiO₂-50 were evaluated using an atomic force microscope, and the corresponding atomic force microscope (AFM) images were shown in Figure 6a,d (see the built-in images). The tested surface roughness of SiO₂ microspheres and SiO₂-TiO₂ were 1.63 and 18.4 nm, respectively. These results show that the surface roughness of SiO₂ increased significantly after it was coated by nano-TiO₂, indicating that the surface structure of SiO₂ has changed. Additionally, in the magnification image of SiO₂-TiO₂ shown in Figure 6b, the nano-TiO₂ particles not only uniformly coated the surface of the SiO₂ microspheres, but also exist in the gap among SiO₂ microspheres. In this way, several microspheres were connected together as a whole.

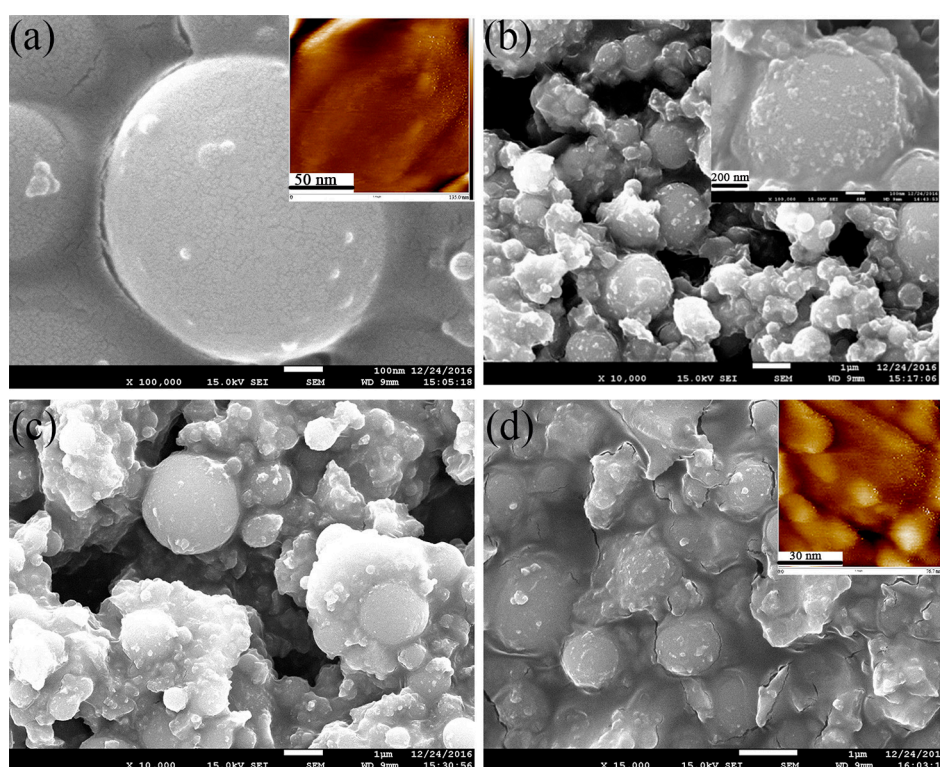


Figure 6. Scanning electron microscope (SEM) and atomic force microscope (AFM) images of (a) SiO₂ microsphere and (b–d) SiO₂-TiO₂ with different ratios. (b) 30% TiO₂, and the inset image is a high magnification image; (c) 40% TiO₂; and (d) 50% TiO₂; the inset images in (a,d) are AFM images.

To confirm the composition of the coating on the surface of SiO₂ microsphere, a surface scanning analysis of the main elements in the selected part of the SiO₂-TiO₂ SEM was carried out (Figure 7). The Ti element was almost distributed throughout the scan area, like the distribution of Si element. The distribution density of Ti element is proportional to the TiO₂ ratio. This confirmed that the nano-TiO₂ particles had coated the surface and were distributed in the gap among SiO₂ microsphere. The results were consistent with SEM results (Figure 6).

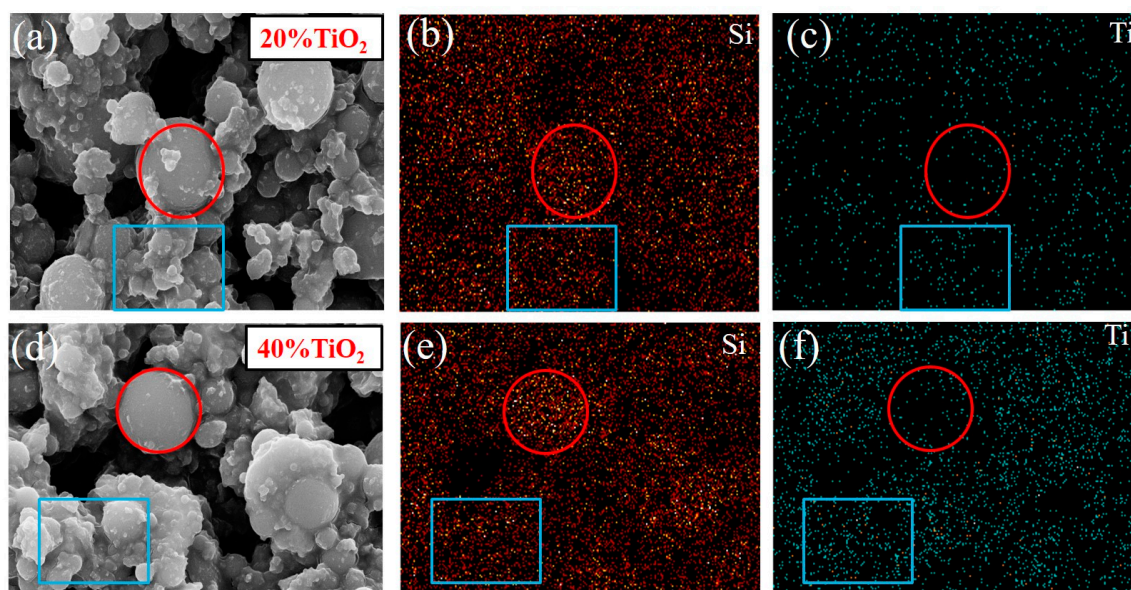


Figure 7. Scanning results of surface elements of $\text{SiO}_2\text{-TiO}_2$ with (a–c) 20% TiO_2 and (d–f) 40% TiO_2 .

Figure 8 shows the TEM and high resolution transmission electron microscopy (HRTEM) images of the $\text{SiO}_2\text{-TiO}_2$ samples (TiO_2 ratio is 40%). Circular SiO_2 microspheres and irregular nano- TiO_2 particles surrounding the SiO_2 microspheres are observed in Figure 8a, confirming that the nano- TiO_2 particles has coated the surface of SiO_2 microspheres. In the HRTEM (Figure 8c), the interplanar spacing of the three major facets were measured to be $d = 0.352 \text{ nm}$ [33], which was consistent with the (101) crystal face of anatase (JCPDS 21-1272). The above results indicated that the nano- TiO_2 coating on the surface of SiO_2 microspheres was anatase and that the mainly exposed crystal face was (101).

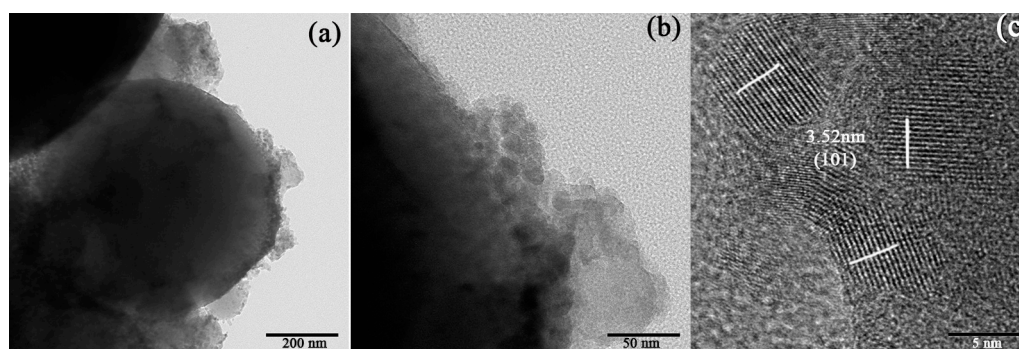


Figure 8. (a,b) Transmission electron microscope (TEM) and (c) high resolution transmission electron microscopy (HRTEM) images of $\text{SiO}_2\text{-TiO}_2$ at different scales.

3.3. Mechanism of the Interaction between SiO_2 and TiO_2 Particles

Figure 9 shows the FT-IR spectra of SiO_2 and $\text{SiO}_2\text{-TiO}_2$ with different TiO_2 ratios. The absorption bands at 1115 , 808 , and 477 cm^{-1} are typical absorption bands of Si–O bonds, indicating that the main component of the composite is SiO_2 [34]. With the increase in the TiO_2 ratio, the intensity of absorption bands corresponding to SiO_2 decreased, indicating that the nano- TiO_2 coated the SiO_2 surface. In addition, the absorption bands ($3200\text{--}3550 \text{ cm}^{-1}$) derived from Si–OH and Ti–OH showed the significant displacement and broadening phenomena when the SiO_2 was coated by the nano- TiO_2 , indicating that the chemical environment had been changed and the association degree of hydroxyl groups on particles surface had increased. It was obviously caused by the formation of hydrogen

bonds between Si–OH and Ti–OH or the further dehydroxylation reaction. It should be inferred that the chemical combination between SiO₂ microspheres and nano-TiO₂ particles was formed through the interaction of hydroxyl groups on their surfaces.

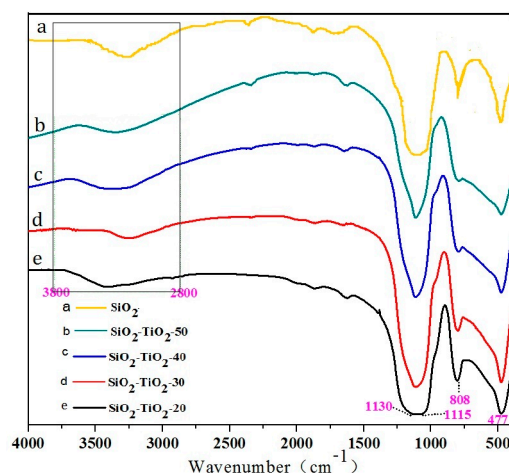


Figure 9. FT-IR of SiO₂–TiO₂ with different TiO₂ ratios. SiO₂–TiO₂-20, 30, 40, 50 represent the mass ratio of TiO₂ to SiO₂–TiO₂ is 20%, 30%, 40% and 50%; The black rectangle region represents the absorption peak caused by the vibration of the hydroxyl radical.

Figure 10 shows the schematic diagram of the bonding mechanism of SiO₂–TiO₂. Based on the above results, the bonding mechanism can be described as follows: firstly, the SiO₂ microspheres were ground in the ethanol medium with grinding balls. The strong grinding force made SiO₂ microspheres depolymerization and exposed more hydroxyl groups, thus displaying the higher reactivity. Secondly, the prepared nano-TiO₂ soliquid was ground with the activated SiO₂ violently, so that the collision probability between particles increased and lead to the contact and reactions between the hydroxyl groups on the SiO₂ and TiO₂ surfaces. Finally, water produced by the dehydroxylation of the particles was further removed by calcination. The SiO₂ and TiO₂ particles were bounded by –Si–O–Ti– bonds. The strength of the chemical bond was stronger than that of van der Waals forces and other physical forces, so the coating of nano-TiO₂ on SiO₂ surface was firm.

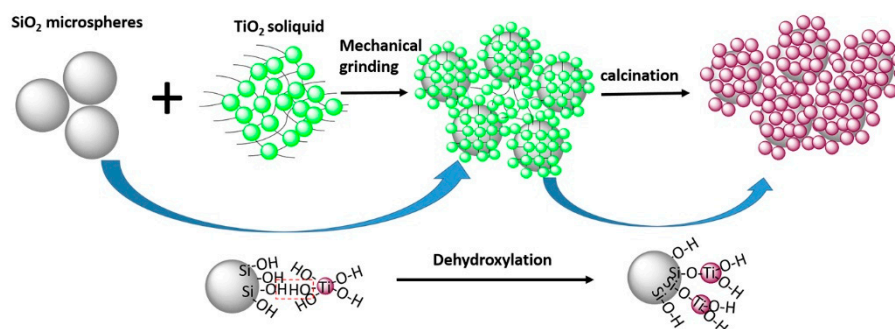


Figure 10. Schematic diagram of the bonding mechanism of SiO₂–TiO₂.

4. Conclusions

In the study, with the by-product SiO₂ microspheres produced during the industry production of fused-zirconia as the substrates, SiO₂–TiO₂ particles were prepared by the wet-grinding of SiO₂ microspheres and nano-TiO₂ and calcination of the ground product. The degradation efficiency of SiO₂–TiO₂ on methyl orange reached 97%, which was significantly higher than that of pure nano-TiO₂.

The water contact angle of SiO₂-TiO₂ was 8°, indicating the strong photoinduced hydrophilicity and the good self-cleaning effect.

The SiO₂-TiO₂ particles were characterized by the nano-TiO₂ uniformly coated on the SiO₂ microspheres and distributed in the microsphere gap. The nano-TiO₂ particles existed in an anatase phase with the particle size of 15–20 nm and are combined with SiO₂ microspheres by the dehydration of hydroxyl groups on particle surfaces.

Author Contributions: Hao Ding, Tongrong Deng and Sijia Sun conceived and designed the experiments; Sijia Sun and Tongrong Deng performed the experiments; Sijia Sun, Tongrong Deng and Wanting Chen analyzed the data; Ying Chen contributed reagents/materials/analysis tools; Sijia Sun and Hao Ding wrote the paper. Authorship must be limited to those who have contributed substantially to the work reported.

Conflicts of Interest: The authors declare no conflict of interest.

References

1. Liu, L.; Chen, X. Titanium dioxide nanomaterials: Self-structural modifications. *Chem. Rev.* **2014**, *114*, 9890–9918. [[CrossRef](#)] [[PubMed](#)]
2. Kormann, C.; Bahnmann, D.W.; Hoffmann, M.R. Preparation and characterization of quantum-size titanium dioxide. *J. Phys. Chem. C* **1988**, *92*, 5196–5201. [[CrossRef](#)]
3. Pu, S.; Zhu, R.; Ma, H.; Deng, D.; Pei, X.; Qi, F.; Chu, W. Facile in-situ design strategy to disperse TiO₂ nanoparticles on graphene for the enhanced photocatalytic degradation of rhodamine 6G. *Appl. Catal. B Environ.* **2017**, *218*, 208–219. [[CrossRef](#)]
4. Preethi, L.K.; Mathews, T.; Nand, M.; Jha, S.N.; Gopinath, C.S.; Dash, S. Band alignment and charge transfer pathway in three phase anatase-rutile-brookite TiO₂, nanotubes: An efficient photocatalyst for water splitting. *Appl. Catal. B Environ.* **2017**, *218*, 9–19. [[CrossRef](#)]
5. Ye, Z.; Tai, H.; Guo, R.; Yuan, Z.; Liu, C.; Su, Y.; Chen, Z.; Jiang, Y. Excellent ammonia sensing performance of gas sensor based on graphene/titanium dioxide hybrid with improved morphology. *Appl. Surf. Sci.* **2017**, *419*, 84–90. [[CrossRef](#)]
6. Fu, H.; Yang, X.; An, X.; Fan, W.; Jiang, X.; Yu, A. Experimental and theoretical studies of V₂O₅@TiO₂ core-shell hybrid composites with high gas sensing performance towards ammonia. *Sens. Actuators B Chem.* **2017**, *252*, 103–115. [[CrossRef](#)]
7. Jalvo, B.; Faraldos, M.; Bahamonde, A.; Rosal, R. Antimicrobial and antibiofilm efficacy of self-cleaning surfaces functionalized by TiO₂ photocatalytic nanoparticles against staphylococcus aureus and pseudomonas putida. *J. Hazard. Mater.* **2017**, *340*, 160–170. [[CrossRef](#)] [[PubMed](#)]
8. Tan, B.Y.L.; Tai, M.H.; Juay, J.; Liu, Z.; Sun, D. A study on the performance of self-cleaning oil-water separation membrane formed by various TiO₂, nanostructures. *Sep. Purif. Technol.* **2015**, *156*, 942–951. [[CrossRef](#)]
9. Ganesh, V.A.; Raut, H.K.; Nair, A.S.; Ramakrishna, S. A review on self-cleaning coatings. *J. Mater. Chem. A* **2011**, *21*, 16304–16322. [[CrossRef](#)]
10. Kim, S.M.; In, I.; Park, S.Y. Study of photo-induced hydrophilicity and self-cleaning property of glass surfaces immobilized with TiO₂ nanoparticles using catechol chemistry. *Surf. Coat. Technol.* **2016**, *294*, 75–82. [[CrossRef](#)]
11. Petica, A.; Gaidau, C.; Ignat, M.; Sendrea, C.; Anicai, L. Doped TiO₂ nanophotocatalysts for leather surface finishing with self-cleaning properties. *J. Coat. Technol. Res.* **2015**, *12*, 1153–1163. [[CrossRef](#)]
12. Diamanti, M.V.; Paolini, R.; Rossini, M.; Aslan, A.B.; Zinzi, M.; Poli, T.; Pedeferrri, M.P. Long term self-cleaning and photocatalytic performance of anatase added mortars exposed to the urban environment. *Constr. Build. Mater.* **2015**, *96*, 270–278. [[CrossRef](#)]
13. Rao, X.; Liu, Y.; Fu, Y.; Liu, Y.; Yu, H. Formation and properties of polyelectrolytes/TiO₂ composite coating on wood surfaces through layer-by-layer assembly method. *Holzforschung* **2016**, *70*, 361–367. [[CrossRef](#)]
14. Lei, M.; Li, F.S.; Tanemura, S.; Fisher, C.A.J.; Li, L.Z.; Liang, Q.; Xu, G. Cost-effective nanoporous SiO₂-TiO₂, coatings on glass substrates with antireflective and self-cleaning properties. *Appl. Energy* **2013**, *112*, 1198–1205.

15. Diamanti, M.V.; Gadelrab, K.R.; Pedefferri, M.P.; Stefancich, M.; Pehkonen, S.O.; Chiesa, M. Nanoscale investigation of photoinduced hydrophilicity variations in anatase and rutile nanopowders. *Langmuir* **2013**, *29*, 14512–14518. [[CrossRef](#)] [[PubMed](#)]
16. Calia, A.; Lettieri, M.; Masieri, M. Durability assessment of nanostructured TiO₂ coatings applied on limestones to enhance building surface with self-cleaning ability. *Build. Environ.* **2016**, *110*, 1–10. [[CrossRef](#)]
17. Jo, W.K.; Tayade, R.J. Facile photocatalytic reactor development using nano-TiO₂ immobilized mosquito net and energy efficient UVLED for industrial dyes effluent treatment. *J. Environ. Chem. Eng.* **2016**, *4*, 319–327. [[CrossRef](#)]
18. Natarajan, K.; Natarajan, T.S.; Tayade, R.J. Photocatalytic reactor based on UV-LED/TiO₂ coated quartz tube for degradation of dyes. *Chem. Eng. J.* **2011**, *178*, 40–49. [[CrossRef](#)]
19. Yang, S.B.; Chun, H.H.; Tayade, R.J.; Jo, W.K. Iron-functionalized titanium dioxide on flexible glass fibers for photocatalysis of benzene, toluene, ethylbenzene, and *o*-xylene (BTEX) under visible- or ultraviolet-light irradiation. *J. Air Waste Manag.* **2015**, *65*, 365–373. [[CrossRef](#)] [[PubMed](#)]
20. Smitha, V.S.; Manjumol, K.A.; Baiju, K.V.; Ghosh, S.; Perumal, P.; Warriar, K.G.K. Sol–gel route to synthesize titania-silica nano precursors for photoactive particulates and coatings. *J. Sol-Gel Sci. Technol.* **2010**, *54*, 203–211. [[CrossRef](#)]
21. Shi, G.; Chen, J.; Wang, L.; Wang, D.; Yang, J.; Li, Y.; Zhang, L.; Ni, C.; Chi, L. Titanium oxide/silicon moth-eye structures with antireflection, p–n heterojunctions and superhydrophilicity. *Langmuir* **2016**, *32*, 27666724. [[CrossRef](#)] [[PubMed](#)]
22. Pakdel, E.; Daoud, W.A. Self-cleaning cotton functionalized with TiO₂/SiO₂ focus on the role of silica. *J. Colloid Interface Sci.* **2013**, *401*, 1–7. [[CrossRef](#)] [[PubMed](#)]
23. Prabhu, S.; Cindrella, L.; Kwon, O.J.; Mohanraju, K. Superhydrophilic and self-cleaning RGO–TiO₂, composite coatings for indoor and outdoor photovoltaic applications. *Sol. Energy Mater. Sol. Cells* **2017**, *169*, 304–312. [[CrossRef](#)]
24. Zhou, J.; Tan, Z.; Liu, Z.; Jing, M.; Liu, W.; Fu, W. Preparation of transparent fluorocarbon/TiO₂–SiO₂, composite coating with improved self-cleaning performance and anti-aging property. *Appl. Surf. Sci.* **2017**, *396*, 161–178. [[CrossRef](#)]
25. Zhang, H.; Fan, D.; Yu, T.; Wang, C. Characterization of anti-reflective and self-cleaning SiO₂–TiO₂, composite film. *J. Sol-Gel Sci. Technol.* **2013**, *66*, 274–279. [[CrossRef](#)]
26. Ciprian, M.; Alexandru, E.; Anca, D. SiO₂/TiO₂ multi-layered thin films with self-cleaning and enhanced optical properties. *Bull. Mater. Sci.* **2017**, *40*, 1–10. [[CrossRef](#)]
27. Surolia, P.K.; Tayade, R.J.; Jasra, R.V. TiO₂-coated cenospheres as catalysts for photocatalytic degradation of methylene blue, *p*-nitroaniline, *n*-decane, and *n*-tridecane under solar irradiation. *Ind. Eng. Chem. Res.* **2010**, *49*, 8908–8919. [[CrossRef](#)]
28. Mavukkandy, M.O.; Bilad, M.R.; Kujawa, J.; Al-Gharabli, S.; Arafat, H.A. On the effect of fumed silica particles on the structure, properties and application of PVDF membranes. *Sep. Purif. Technol.* **2017**, *187*, 365–373. [[CrossRef](#)]
29. Peng, Y.; Zhang, J.; Liu, J.; Ke, J.; Wang, F. Properties and microstructure of reactive powder concrete having a high content of phosphorous slag powder and silica fume. *Constr. Build. Mater.* **2015**, *101*, 482–487. [[CrossRef](#)]
30. Pedro, D.; Brito, J.D.; Evangelista, L. Mechanical characterization of high performance concrete prepared with recycled aggregates and silica fume from precast industry. *J. Clean. Prod.* **2017**, *164*, 939–949. [[CrossRef](#)]
31. Liu, J.; Wang, D. Influence of steel slag-silica fume composite mineral admixture on the properties of concrete. *Powder Technol.* **2017**, *320*, 230–238. [[CrossRef](#)]
32. Wang, S.; Zheng, W.T.; Lian, J.S.; Jiang, Q. Photocatalytic property of Fe doped anatase and rutile TiO₂ nanocrystal particles prepared by sol–gel technique. *Appl. Surf. Sci.* **2012**, *263*, 260–265. [[CrossRef](#)]
33. Zhou, X.; Wu, J.; Zhang, J.; He, P.; Ren, J.; Zhang, J.; Lu, J.; Liang, P.; Xu, K.; Shui, F. The effect of surface heterojunction between (001) and (101) facets on photocatalytic performance of anatase TiO₂. *Mater. Lett.* **2017**, *205*, 173–177. [[CrossRef](#)]
34. Chen, Y.; Ding, H.; Sun, S. Preparation and characterization of ZnO nanoparticles supported on amorphous SiO₂. *Nanomaterials* **2017**, *7*, 217. [[CrossRef](#)] [[PubMed](#)]

